J Optim Theory Appl (2016) 168:534–550
DOI 10.1007/s10957-015-0816-7

Numerical Solution of a Class of Moving Boundary Problems with a Nonlinear Complementarity Approach

Grigori Chapiro[1] · Angel E. R. Gutierrez[2] · José Herskovits[3,4] · Sandro R. Mazorche[1] · Weslley S. Pereira[1]

Received: 22 April 2015 / Accepted: 22 September 2015 / Published online: 5 October 2015

Abstract Parabolic-type problems, involving a variational complementarity formulation, arise in mathematical models of several applications in Engineering, Economy, Biology and different branches of Physics. These kinds of problems present several analytical and numerical difficulties related, for example, to time evolution and a moving boundary. We present a numerical method that employs a global convergent nonlinear complementarity algorithm for solving a discretized problem at each time step. Space discretization was implemented using both the finite difference implicit scheme and the finite element method. This method is robust and efficient. Although the present method is general, at this stage we only apply it to two one-dimensional examples. One of them involves a parabolic partial differential equation that describes oxygen diffusion problem inside one cell. The second one corresponds to a system of nonlinear differential equations describing an in situ combustion model. Both models are rewritten in the quasi-variational form involving moving boundaries. The numerical results show good agreement when compared to direct numerical simulations.

Communicated by Ilio Galligani.

✉ Grigori Chapiro
grigori@ice.ufjf.br

1 Department of Mathematics, Federal University of Juiz de Fora, Juiz de Fora, Brazil

2 Instituto de Matemática y Ciencias Afines (IMCA), Lima, Peru

3 Department of Mechanical and Materials Engineering, Military Institute of Engineering, Rio de Janeiro, Brazil

4 Mechanical Engineering Program, COPPE, Federal University of Rio de Janeiro, Rio de Janeiro, Brazil

Keywords Moving boundary problems · Nonlinear complementarity algorithms · Combustion · Diffusion

Mathematics Subject Classification 35R37 · 90C33 · 80A25

1 Introduction

Parabolic problems that can be written as a variational problem involving a complementarity condition and moving boundaries appear in several applications; see [1]. In [2], several examples in Engineering and Economics are described. We propose a general technique for moving boundary problems that can be written as the complementarity problem and implement it for the one-dimensional case.

The numerical method is based on a combination of the Crank–Nicolson finite difference scheme [3] and a globally convergent nonlinear complementarity algorithm (FDA-NCP) [4]. As a result, the moving boundary is obtained naturally, without need of regularizations unlike from other methods. The robustness of the algorithm allows longer time steps as shown in our preliminary results; see [5]. Other methods dealing with complementarity problems can be found in [4,6–8]. The present technique is appropriate for practical applications since it brings together classical numerical techniques for PDEs with a robust and efficient interior point algorithm for nonlinear complementarity problems, having a complete theoretical fundamentation and good numerical results.

This paper is organized as follows. In Sect. 2, we describe the complementarity algorithm employed at each time step and the finite difference scheme used for time evolution. In Sect. 3, we introduce the physical model of oxygen diffusion and describe numerical results comparing them with the existing data. In Sect. 4, we introduce the model describing in situ combustion and study rigorously the non-combustion waves. In Sect. 5, we present numerical results for in situ combustion using FDS and MEF. Finally, in Sect. 6, we present some conclusions and discussions.

2 The Numerical Method

In this section, we describe our approach to solve the system of parabolic partial differential equations numerically. The problem consists in finding $u(x,t) : I \times \mathbb{R}_+ \to \mathbb{R}^n$ and the moving boundary $s(t) : \mathbb{R}_+ \to \mathbb{R}$ such that

$$F(u) = 0, \ \text{for}\, x < s(t); \quad \text{and} \quad u = 0, \ \text{for}\, x \geq s(t), \tag{1}$$

where $F(u) : \mathbb{R}^n \to \mathbb{R}^n$ and the interval I can be $\mathbb{R}$, $\mathbb{R}_+$ or a compact interval. We study the case when Eq. (1) can be written as the complementarity problem using Hadamard product "$\circ$,"

$$F(u) \geq 0, \quad u \geq 0 \quad \text{and} \quad u \circ F(u) = 0. \tag{2}$$

Several examples where (1) and (2) are equivalent can be found in [9].

We use FDS and FEM for space discretization and a nonlinear complementarity algorithm to solve the discrete problem at each time step. In this way, the implementation is flexible, since we can change the space discretization and the algorithm independently. Next we present a brief description of the algorithm FDA-NCP.

2.1 The Nonlinear Complementarity Algorithm

Let $F : D \subset \mathbb{R}^n \to \mathbb{R}^n$ be a nonlinear vector function. The nonlinear complementarity problem consists in finding $u \in \mathbb{R}^n$ satisfying (2), where $u \geq 0$ means that each component of the vector u is nonnegative. We call $\Upsilon = (u \in \mathbb{R}^n : u \geq 0, F(u) \geq 0)$ the feasible set and $\text{int}(\Upsilon)$ its interior.

FDA-NCP is an iterative algorithm to solve problem (2). It starts from an initial point in $\text{int}(\Upsilon)$ and generates a sequence of points also in $\text{int}(\Upsilon)$ that converges to the required solution. At each point, it defines a feasible direction that is also a descent direction for the potential function $\Phi(u) = \sum_{i=1}^{n} u_i \, F_i(u)$. On that direction, a new interior point with a lower potential is obtained. This point is defined to be the next point of the sequence, and the algorithm returns to the first step till a convergence criterion is satisfied. The search direction is based on Newton's direction for the nonlinear system of equations $u \circ F(u) = 0$. To obtain feasibility, Newton's direction is modified by a restoration direction, as done in [10]. The present approach is supported by strong theoretical results [11].

The following notation will be employed to describe the algorithm FDA-NCP: $F^k = F(u^k)$, $M^k = \nabla(u^k \circ F(u^k))$, $\Phi^k = \Phi(u^k)$, $\nabla\Phi^k = \nabla\Phi(u^k)$ and $\mu^k = \Phi^k/n$.

FDA-NCP Algorithm

Data: $u^0 \in \text{int}(\Upsilon)$, $k = 0$, $\epsilon > 0$, $E = [1, \ldots, 1]^T$, $\nu, \nu_1 \in]0, 1[$, $\alpha \in]0, 1/2[$.

Step 1: Compute the search direction d^k by solving $M^k \, d^k = -u^k \circ F^k + \alpha \, \mu^k \, E$.

Step 2: Armijo line search. Set t^k as the first number in the sequence $1, \nu, \nu^2, \nu^3, \ldots$ that satisfies:

$u^k + t^k \, d^k \geq 0$, $F(u^k + t^k \, d^k) \geq 0$ and $\Phi(u^k + t^k \, d^k) \geq \Phi^k + t^k \, \nu_1 \, (\nabla\Phi^k . d^k)$.

Step 3: Update. Set $u^{k+1} = u^k + t^k \, d^k$ and $k = k + 1$.

Step 4: Stopping criterion: if $\|u^k \circ F^k\| \leq \epsilon$ stop, else go to step 1.

In [4,11], it has been shown that the search direction d^k is well defined in Υ and the global convergence of FDA-NCP scheme is guaranteed under the following assumptions:

1. The set $\Upsilon_c = (u \in \Upsilon : \Phi(u) < c)$, $c > 0$ is a compact set and has an interior Υ_c^0. Each $u \in \Upsilon_c^0$ satisfies $u > 0$ and $F(u) > 0$.

2. The function $F(u)$ is continuously differentiable and $\nabla F(u)$ satisfies the Lipschitz condition $||\nabla F(w) - \nabla F(u)|| < \gamma_0 ||w - u||$, for any $u, w \in \Upsilon_c$, where γ_0 is a positive real number.

3. The matrix $diag(F(u)) + diag(u)\nabla F(u)$ has an inverse in Υ_c^0.

In [11], it was proved that if $t^k = 1$ for large k the algorithm rate of convergence is quadratic.

2.2 The Present Algorithm

We consider an homogeneous grid for the variable x with $M + 1$ points, where x_0 and x_M are the boundary points of the interval of the calculation. The grid spacing is $h = x_{m+1} - x_m = 1/M$, and the grid position m corresponds to $x = m\Delta x$. Analogously, the time is denoted by t with the time index denoted by n and the time step is Δt. However, we consider adaptive time step finite difference schemes, so Δt may change from one grid level to another and $t = \sum_{i=1}^{n} \Delta t_n$.

In order to solve our problem, we employ the following scheme

Step 0: We start with the initial variable u_m^0, $m = 0, 1, \ldots, M$ and the first time step Δt_0.

Step 1: Obtain the discrete form of Eq. (2) using FDS or FEM.

Step 2: Use FDA-NCP algorithm to solve the complementarity problem from **step 1**.

Step 3: Use the solution from **step 2** as the variable u value at the next time step.

Repeat the algorithm from the **step 1** until reaching the final time.

The global properties of the Crank–Nicolson scheme are well known, e.g., [12]. In general, the convergence of FDS and FEM is rigorously proved only for simple equations or linear systems; see [3], and however, they are widely used for solving numerically reaction–diffusion equations similar to the examples addressed here [5, 13–16].

3 The Oxygen Diffusion Problem

Here we study the particular case of one-dimensional oxygen diffusion that involves a moving boundary. For simplicity, the oxygen is allowed to diffuse into a medium that consumes oxygen at constant rate. The concentration of oxygen at the surface of the medium is kept constant. A moving boundary marks the limit of oxygen penetration.

The major challenge is that of tracking the movement of the boundary during this stage of the process as well as determining the distribution of oxygen throughout the medium at any instant. This type of problem is known as an implicit moving boundary problem; see [1]. Several analytical and numerical methods were employed to solve this problem. We mention [15–21] and references therein.

The process takes place in two phases. The first one evolves until a steady state, without oxygen transfer into the medium, is attained. At the second phase, the surface of the medium is sealed so that no more oxygen passes in or out. The medium continues consuming the oxygen already diffusing in it, and as a consequence, the boundary marking the depth of penetration in the steady state recedes toward the sealed surface.

Following [1,5], the system of partial differential equations describing this problem can be written in non-dimensional form:

$$\frac{\partial c}{\partial t} = \frac{\partial^2 c}{\partial x^2} - 1, \quad 0 \le x \le s(t), \tag{3}$$

$$\frac{\partial c}{\partial x} = 0, \quad x = 0, \quad 0 < t, \tag{4}$$

$$c = \frac{\partial c}{\partial x} = 0, \quad x = s(t), \quad 0 < t, \tag{5}$$

$$c = \frac{1}{2}(1-x)^2, \quad 0 \le x \le 1, \quad t = 0, \tag{6}$$

where $c(x,t) \ge 0$ is the concentration of oxygen free to diffuse and $s(t)$ is the value of x separating regions where $c = 0$ and $c > 0$. Eq. (3) represents the PDE at the left side of the moving boundary, Eqs. (4) and (5) represent the boundary conditions, and Eq. (6) is the initial condition.

Following [15], System (3)–(6) can be rewritten into a variational formulation in the form of Eq. (2).

$$\frac{\partial c}{\partial t} - \frac{\partial^2 c}{\partial x^2} + 1 \ge 0, \quad c \ge 0, \quad \left(\frac{\partial c}{\partial t} - \frac{\partial^2 c}{\partial x^2} + 1\right) c = 0, \tag{7}$$

where the boundary and the initial conditions are defined by (4) and (6), respectively. The first inequality in (7) is satisfied as equality by (3) inside the region $0 < x < s(t)$. When $s(t) \le x \le 1$ by (5), we get $c = 0$, and thus, (7) is valid. The inequality $c \ge 0$ follows from (6). The equality in (7) is valid because for any $x \in [0,1]$ one of the factors vanishes.

The equivalence between the solution of the system of equations in the variational approach (7) and the weak solution of the Stefan problem described by System (3)–(6) was locally studied in [22] and [23].

3.1 Numerical Implementation and Results

Next we implement the oxygen diffusion problem using Crank–Nicolson FDS and describe the numerical results. Let be $F(c)$ the differential operator corresponding to the left side of the first inequality in (7). Then, in discrete form, we have

$$F_{\Delta}(c) = \frac{c_m^{n+1} - c_m^n}{\Delta t} - \frac{c_{m-1}^{n+1} - 2c_m^{n+1} + c_{m+1}^{n+1}}{2\Delta x^2} - \frac{c_{m-1}^{n} - 2c_m^{n} + c_{m+1}^{n}}{2\Delta x^2} + 1. \tag{8}$$

Substituting the differential operator $F(c)$ in (7) by the discrete operator $F_{\Delta}(c)$, multiplying the inequality by Δt and isolating the terms for time step $n+1$ on the left we obtain:

$$-\frac{\mu}{2}c_{m-1}^{n+1} + (1+\mu)c_m^{n+1} - \frac{\mu}{2}c_{m+1}^{n+1} \ge \frac{\mu}{2}c_{m-1}^{n} + (1-\mu)c_m^{n} + \frac{\mu}{2}c_{m+1}^{n} - \Delta t, \tag{9}$$

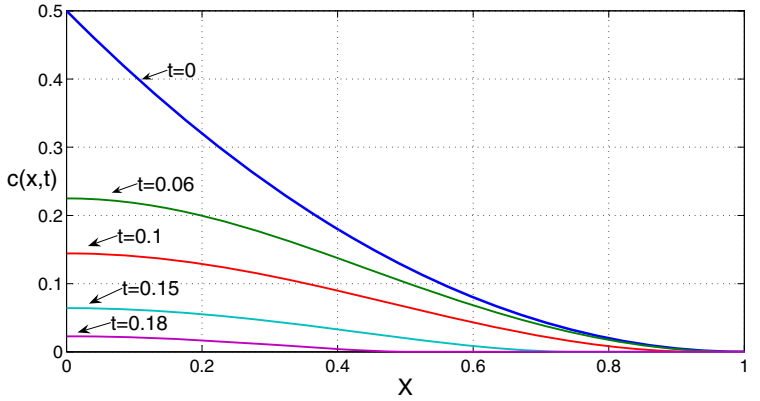

Fig. 1 Results of the second phase of the oxygen diffusion problem

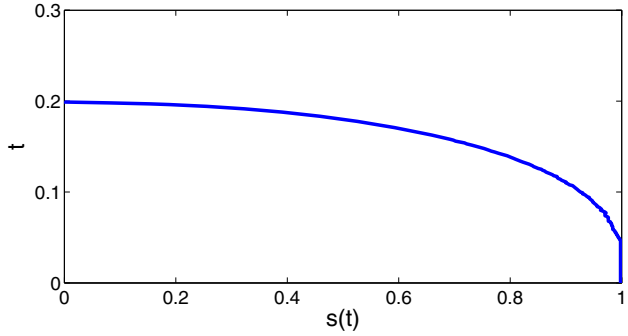

Fig. 2 Moving boundary position $s(t)$ on the *horizontal* coordinate and time t on the *vertical* one

where $\mu = \Delta t/\Delta x^2$. The evaluation equations for the grid points $m = 0$ and $m = M$ can be described in similar way assuming Neumann zero flow boundary conditions; see [3].

We start with the equilibrium solution as initial conditions and use Neumann boundary conditions at the left and right sides of the interval $\partial c/\partial x(x_0) = 0$ and $\partial c/\partial x(x_N) = 0$. The results plotted in Fig. 1 are very similar to those shown in Fig. 3 of [15], where semi-analytical techniques were employed.

Finally, we can describe the moving boundary position $s(t)$ as a function of time as shown in Fig. 2, and it is visually identical to one in [15]. Our numerical results show good agreement with the literature as described in Table 1.

4 In Situ Combustion

In this section, we address a simple in situ combustion model described by a system of two nonlinear differential equations. We consider the situation when the porous medium initially contains solid fuel and oxygen. There are many analytical studies of combustion waves in high-temperature regimes, e.g., [14,25,26] and references

Table 1 Moving boundary position

Time	CN-cub	CN-lin	CSBT	A	HH	CG	G	GK
0.0	1.0000	1.0000	1.0000	1.0000	1.00000	–	–	–
0.02	1.0000	1.0000	1.0000	0.9992	1.00000	–	–	–
0.04	1.0000	1.0000	1.0000	0.9983	0.99918	0.9988	0.9988	0.9950
0.06	0.9840	0.9935	0.9900	0.9921	0.99918	0.9905	0.9903	0.9899
0.08	0.9640	0.9729	0.9620	0.9663	0.97155	0.9650	0.9613	0.9623
0.10	0.9303	0.9400	0.9260	0.9313	0.93501	0.9312	0.9301	0.9249
0.12	0.8730	0.8799	0.8720	0.8750	0.87916	0.8747	0.8719	0.8703
0.14	0.7928	0.8004	0.7940	0.7937	0.79891	0.7912	0.7882	0.7916
0.16	0.6748	0.6880	0.6780	0.6784	0.68337	0.6756	0.6682	0.6825
0.18	0.4942	0.5042	0.5000	0.4909	0.50109	0.4849	0.4766	0.4768
0.19	0.3419	0.3509	0.3520	0.3401	0.34537	–	–	–
0.195	0.2049	0.2193	0.2340	0.2012	0.20652	–	–	–

In this table, we compare the results of the present work to: A: [17]; HH: [21]; CG: [15]; G: [24]; GK: [16]. CN-cub and CN-lin correspond to Crank–Nicolson scheme with cubic and linear interpolation, and CSBT corresponds to implicit central space scheme with cubic interpolation

therein. As in [13], we focus on the case when the reaction is active for all temperatures. In our simplified model, we consider that only a small part of the available space is occupied by the fuel, so that changes in porosity in the reaction are negligible. We assume that pressure variations are small compared to prevailing pressure yielding constant gas speed and local thermal equilibrium; i.e., the temperatures of solid and gas are the same. Heat losses are neglected, which is reasonable for in situ combustion in field conditions. We consider unlimited quantity of oxygen. This is exactly the situation that happens in self-propagating high-temperature synthesis (SHS); see [27].

We propose a simplified model derived from [13,25] under the assumptions described above. It includes the heat balance Eq. (10), the molar balance equations for fuel and the ideal gas law (11)

$$C_m \frac{\partial T}{\partial t} + \frac{\partial (c_g \rho u (T - T_{\text{res}}))}{\partial x} = \lambda \frac{\partial^2 T}{\partial x^2} + Q_r W_r, \tag{10}$$

$$\frac{\partial \rho_f}{\partial t} = -\mu_f W_r, \quad T = P/(\rho R). \tag{11}$$

Here the unknowns are T, ρ and ρ_f, where T $[K]$ is the temperature, ρ [mole/m^3] is the molar density of gas, ρ_f [mole/m^3] is the molar concentration of immobile fuel, t is the time coordinate, and x is the space coordinate. Following [13,25], the system parameters are considered constant and their values are given in Table 2. Systems (10) and (11) have to be solved for $x \in [0, \infty[$ with left boundary condition given by the injection conditions $\rho_f = 0$ and $T = T_{\text{res}}$.

Although several chemical reactions are involved in the combustion process, we consider the simplified case when $C + O_2 \rightarrow CO_2$. Thus, one mole of immobile fuel reacts with one mole of O_2 and generates one mole of gaseous products, yielding

Table 2 Dimensional parameter values for in situ combustion

Symbol	Physical quantity	Value	Unit
T_{res}	Initial reservoir temperature	273	K
C_m	Heat capacity of porous medium	2×10^6	J/m^3 K
c_g	Heat capacity of gas	27.42	J/mole K
λ	Thermal conductivity of porous medium	0.87	J/(m s K)
Q_r	Immobile fuel combustion enthalpy at T_{res}	4×10^5	J/mole
E_r	Activation energy	58000	J/mole
k_p	Pre-exponential parameter	500	1/s
R	Ideal gas constant	8.314	J/(mole K)
P	Prevailing pressure (1 atm)	101325	Pa
u_{inj}	Darcy velocity of injected gas (200 m/day)	2.3×10^{-3}	m/s
ρ_f^{res}	Initial molar density of fuel	372	mole/m^3

$\mu_f = 1$. As in [13,25], the reaction rate W_r for unlimitted oxygen supply will be taken as

$$W_r = k_p \rho_f \exp\left(-E_r/(RT)\right), \tag{12}$$

where typical values of k_p and E_r also are given in Table 2.

To obtain the dimensionless form of System (10)–(11), we introduce dimensionless dependent and independent variables, denoted by tildes, as ratios of the dimensional quantities and reference quantities, denoted by stars

$$\tilde{t} = \frac{t}{t^*},\ \tilde{x} = \frac{x}{x^*},\ \tilde{\theta} = \Delta\tilde{T} = \frac{T - T_{\text{res}}}{\Delta T^*},\ \tilde{\rho} = \frac{\rho}{\rho^*},\ \tilde{\eta} = 1 - \frac{\rho_f}{\rho_f^*},\ \tilde{u} = \frac{u_{\text{inj}}}{u^*}. \tag{13}$$

Our choice for the reference quantities is

$$\begin{aligned} &t^* = Q_r \rho_f^{\text{res}}, \quad \rho^* = P/(RT_{\text{res}}), \quad \Delta T^* = t^*/C_m, x^* = c_g \\ &\rho^* \Delta T^*, \quad \rho_f^* = \rho_f^{\text{res}}, \quad u^* = x^*/t^*, \end{aligned} \tag{14}$$

where T_{res} and ρ_f^{res} are, respectively, the initial reservoir temperature and the molar density of fuel, u_{inj} is the injection gas velocity. In (14), t^* is the characteristic time for fuel combustion at the initial reservoir temperature T_{res} and ΔT^* is the deviation of peak temperature from reservoir temperature, for the case of complete combustion of fuel under adiabatic conditions.

Using (13), (14) and omitting the tildes, Eqs. (10)–(12) are written in dimensionless form as:

$$\frac{\partial \theta}{\partial t} + u \frac{\partial (\rho\theta)}{\partial x} = \frac{1}{\text{Pe}_T} \frac{\partial^2 \theta}{\partial x^2} + \Phi, \tag{15}$$

$$\frac{\partial \eta}{\partial t} = \Phi, \tag{16}$$

$$\rho = \theta_0/(\theta + \theta_0), \tag{17}$$

$$\Phi = \beta(1-\eta)\exp\left(-\frac{\mathcal{E}}{\theta+\theta_0}\right), \tag{18}$$

where θ is the scaled temperature, η represents immobile fuel depth as commonly used in oil engineering ($\eta = 1$ means no fuel and $\eta = 0$ means maximum fuel). Here Pe_T is the Peclet number for thermal diffusion, u is the dimensionless gas speed, $\mathcal{E}$ is the scaled activation energy, and θ_0 is the scaled reservoir temperature. Typical values of the quantities in (15)–(18) are given in Sect. 5. The system must be solved with the initial reservoir conditions

$$t = 0,\ x \geq 0: \quad \theta = 0,\ \ \eta = 0, \tag{19}$$

and the left boundary conditions corresponding to the injection conditions

$$t \geq 0,\ x = 0: \quad \theta = 0,\ \ \eta = 1. \tag{20}$$

In order to represent Systems (15) and (16) in a complementarity form, we make a transformation similar to Sect. 3 (see also [6]), obtaining:

$$\theta \geq 0; \quad \eta \geq 0; \quad \frac{\partial \theta}{\partial t} + u\frac{\partial(\rho\theta)}{\partial x} - \frac{1}{\mathrm{Pe}_T}\frac{\partial^2\theta}{\partial x^2} + \Phi \geq 0; \quad \frac{\partial \eta}{\partial t} - \Phi \geq 0; \tag{21}$$

$$\left(\frac{\partial \theta}{\partial t} + u\frac{\partial(\rho\theta)}{\partial x} - \frac{1}{\mathrm{Pe}_T}\frac{\partial^2\theta}{\partial x^2} + \Phi\right)\theta = 0; \quad \left(\frac{\partial \eta}{\partial t} - \Phi\right)\eta = 0. \tag{22}$$

We need Eq. (22) to be satisfied at the right end of the interval, where Eq. (15) may not be satisfied. This explains the choice of dimensionless variable η describing fuel depth inside the reservoir.

4.1 Non-Combustion Waves

Apart of the combustion wave, the solution of System (15)–(17) possesses non-combustion waves, which can be studied analytically and used to validate numerical simulations. We consider a hyperbolic part of System (15)–(17) obtained by neglecting the reaction terms and second derivatives; see [13] and references therein.

$$\frac{\partial \theta}{\partial t} + u\frac{\partial}{\partial x}\left(\frac{\theta_0\theta}{\theta+\theta_0}\right) = 0, \qquad \frac{\partial \eta}{\partial t} = 0. \tag{23}$$

The equations above form a system of conservation laws and can be solved for the corresponding Riemann problem, i.e., considering the initial data given by the discontinuous step function. Typically, the solution of a Riemann problem is a train

of waves, which can be shocks, rarefaction or contact discontinuities. This solution is physically admissible if it satisfies the entropy conditions; see [28] for details.

Theorem 4.1 *The solution of System* (23) *with initial data given by*

$$(\theta(x,0),\eta(x,0)) = \begin{cases} (\theta_l,\eta_l), & x \leq 0 \\ (\theta_r,\eta_r), & x > 0 \end{cases} \tag{24}$$

where θ_l, η_l, θ_r *and* η_r *are constants satisfying* $\theta_l \leqslant \theta_r$ *can contain:*

(1) *a Lax entropic contact wave satisfying* $\theta_l = \theta_r$ *and* $\eta_r \geq 0$ *with velocity equal to zero;*
(2) *a Lax entropic shock wave satisfying* $\eta_l = \eta_r$ *and* $\theta_r \geq 0$ *with velocity*

$$s = \frac{u\theta_0^2}{(\theta_r+\theta_0)(\theta_l+\theta_0)}. \tag{25}$$

Proof The flux function associated with the system of conservation laws (23) and the corresponding matrix of derivatives are

$$f(\theta,\eta) = \begin{pmatrix} u\dfrac{\theta_0\theta}{\theta+\theta_0} \\ 0 \end{pmatrix} \quad \text{and} \quad f'(\theta,\eta) = \begin{pmatrix} u\dfrac{\theta_0^2}{(\theta+\theta_0)^2} & 0 \\ 0 & 0 \end{pmatrix}. \tag{26}$$

The characteristic functions and characteristic fields of the Jacobian in (26) are given by $\lambda_1 = 0$ and $v_1 = (0,1)^T$; $\lambda_2 = u\theta_0^2/(\theta+\theta_0)^2$ and $v_2 = (1,0)^T$.

Since λ_1 is constant, the first characteristic field is linearly degenerate and the wave that corresponds to this field is an entropic contact discontinuity [28].

Since $\theta \geq 0$, $\rho \geq 0$ and $u > 0$, it follows that the second characteristic field is genuinely nonlinear, i.e.,

$$\lambda_2'(\theta,\eta)\cdot v_2 < 0. \tag{27}$$

Using Rankine–Hugoniot conditions, we obtain the discontinuity propagation velocity s:

$$f(\theta_r,\eta_r) - f(\theta_l,\eta_l) = s\left((\theta_r,\eta_r)^T - (\theta_l,\eta_l)^T\right). \tag{28}$$

Substituting Eq. (26) in (28), after some manipulations we obtain

$$u\theta_0^2\frac{\theta_r-\theta_l}{(\theta_r+\theta_0)(\theta_l+\theta_0)} = s(\theta_r-\theta_l), \quad 0 = s(\eta_r-\eta_l). \tag{29}$$

If $\theta_r = \theta_l$, the discontinuity corresponds to the first characteristic field. It is a contact discontinuity with velocity $s = 0$.

If $\theta_r \neq \theta_l$ then $\eta_r = \eta_l$ and s is given by Eq. (25). This equation verifies Lax entropy condition $\lambda(\theta_l) \geq s \geq \lambda(\theta_r)$. This fact jointly with Eq. (27) implies that the entropic shock discontinuity occurs if and only if $\theta_l < \theta_r$, which is the case of this theorem. □

5 Numerical Solution of In Situ Combustion Model

In this section, we present numerical results using FDA-NCP algorithm and validate the solution obtained with FDS and FEM. The dimensionless parameter values are $\mathrm{Pe}_T = 1406$, $\beta = 7.44 \times 10^{10}$, $\mathcal{E} = 93.8$, $\theta_0 = 3.67$ and $u = 3.76$.

5.1 Numerical Simulation of In Situ Combustion Using FDS

Let be $F(\theta, \eta)$ the differential operator corresponding to the left side of inequality (22). We write it in the discrete form, using Crank–Nicolson scheme:

$$F_\Delta(\theta, \eta) = \left[F^1_\Delta(\theta, \eta), \quad F^2_\Delta(\theta, \eta) \right]^T, \tag{30}$$

where

$$\begin{aligned} F^1_\Delta(\theta, \eta) = {} & \theta^{n+1}_m - \theta^n_m + u\Delta t \frac{\rho^{n+1}_{m+1}\theta^{n+1}_{m+1} - \rho^{n+1}_{m-1}\theta^{n+1}_{m-1}}{4\Delta x} + u\Delta t \frac{\rho^{n}_{m+1}\theta^{n}_{m+1} - \rho^{n}_{m-1}\theta^{n}_{m-1}}{4\Delta x} \\ & - \frac{\Delta t}{\mathrm{Pe}} \frac{\theta^{n+1}_{m-1} - \theta^{n+1}_m + \theta^{n+1}_{m+1}}{2\Delta x^2} - \frac{\Delta t}{\mathrm{Pe}} \frac{\theta^{n}_{m-1} - 2\theta^{n}_m + \theta^{n}_{m+1}}{2\Delta x^2} \\ & - \frac{\Delta t \left(\Phi^{n+1}_m + \Phi^n_m \right)}{2}, \end{aligned} \tag{31}$$

$$F^2_\Delta(\theta, \eta) = \eta^{n+1}_m - \eta^n_m + \frac{\Delta t \left(\Phi^{n+1}_m + \Phi^n_m \right)}{2}. \tag{32}$$

Same discretization was employed in [13,29] to simulate more general and complex combustion models. Goods results were obtained when compared to analytical solutions.

Substituting the differential operator $F(\theta, \eta)$ in (22) by the discrete operator $F_\Delta(\theta, \eta)$ and isolating the terms for time step $n + 1$ on the left, we obtain the system of equations describing time evolution. The evaluation equation for the grid points $m = 0$ and $m = M$ can be described using the boundary conditions.

The boundary conditions impose constant temperature and no fuel at the left end of the interval, $x_0 = 0$. That is $\theta(x_0, t) = 0$ and $\eta(x_0, t) = 1, t \geq 0$. As there is no fixed right point, the boundary conditions at the right are modeled as zero flow Neumann boundary conditions.

To compare the nonlinear complementarity algorithm with the classical Crank–Nicolson scheme, three different simulations were performed inside the interval $[0, 0.05]$ using constant time step k and space grids with 51 ($k = 10^{-5}$), 101 ($k = 5 \times 10^{-6}$) and 201 ($k = 2.5 \times 10^{-6}$) points; see Fig. 3b–d. In Fig. 3, we show the simulations using the algorithm proposed in Sect. 2.1 (lines) and compare it to the same simulation performed by using classical Crank–Nicolson scheme (circles).

As one can see in Fig. 3b for sparse grid, the proposed algorithm shows better results than the finite difference scheme with Newton's method. In Fig. 3b, the simulation with Newton's method and 51-point grid shows dispersion effect. This effect increases

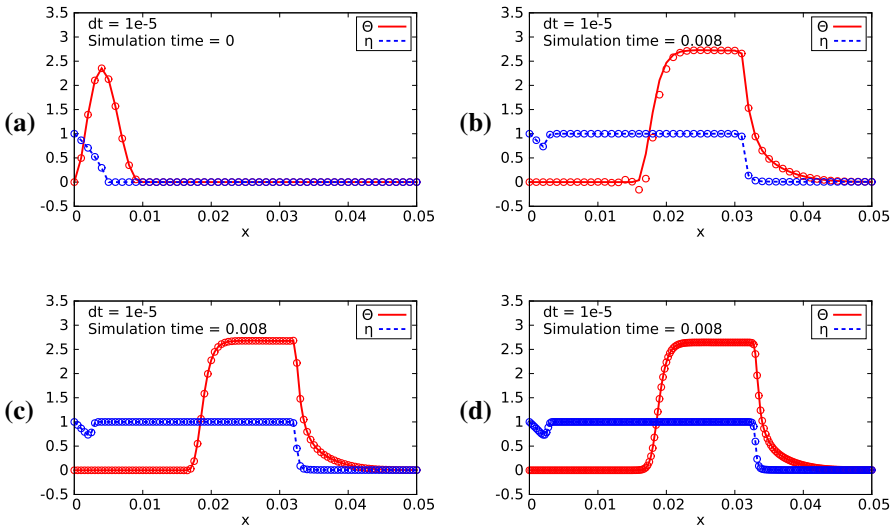

Fig. 3 Solution obtained by using FDS + FDA-NCP (*lines*) is compared to one obtained with Crank–Nicolson + FDS (*circles*). Initial conditions are plotted in (**a**). Solutions at time $t = 0.01$ are shown in (**b**), (**c**) and (**d**) corresponding to grids with 51, 101 and 201 points

Table 3 Relative errors for simulations using FDS

Method	Variable	Error 1	Error 2	Error 3
FDA	θ/η	1.741/0.845	0.977/0.506	0.190/0.230
CN + Newton	θ/η	1.370/0.845	0.974/0.506	0.190/0.230

See text for more details

when more sparse grid is used turning Newton's method divergent. On the other hand, the technique using FDA-NCP converges even with 27-point grid.

Notice that in our simulations the space grid with 101 and 201 points contain all the points used in 51-point grid. Thus, in order to test the convergence of the numerical scheme proposed in Sect. 2.1, we transform the solutions obtained by using the 101- and 201-point grid to 51 points and calculate the Euclidean norm difference at time $t = 0.008$. The results can be seen in Table 3, where the columns *"Error 1," "Error 2"* and *"Error 3"* represent the difference between solutions corresponding to 101- and 51-point grids, 201- and 101-point grids, 401- and 201-point grids, respectively. For comparison, we perform the same analysis for Crank–Nicolson scheme, and the results are shown in the same table. Table 3 shows clear evidence of linear convergence of the method proposed here.

5.2 Numerical Simulation of In Situ Combustion Using FEM

Here we consider System (15)–(18) in $\Omega = [0, 0.05]$ with homogeneous Dirichlet and Neumann boundary conditions for θ in $x = 0$ and $x = 0.05$, respectively. The

initial conditions θ_0 and η_0 are plotted in Fig. 3a. Using standard Galerkin procedure [30], the weak formulation at each time, t, is: find (θ, η) such that

$$\left\langle \frac{\partial \theta}{\partial t}, v \right\rangle - V_T \bar{u} \left\langle \rho\theta, \frac{\partial v}{\partial x} \right\rangle + \frac{1}{\mathrm{Pe}_T} \left\langle \frac{\partial \theta}{\partial x}, \frac{\partial v}{\partial x} \right\rangle - \langle \Phi, v \rangle = 0, \quad \forall v \in H_D^1(\Omega) \tag{33}$$

$$\left\langle \frac{\partial \eta}{\partial t}, w \right\rangle - \langle \Phi, w \rangle = 0, \quad \forall w \in L^2(\Omega) \tag{34}$$

where $H_D^1(\Omega) = \{v \in H_D^1(\Omega);\ v(0) = 0\}$ and $\langle \cdot, \cdot \rangle$ denotes the usual inner product in $L^2(\Omega)$. Notice that in consequence of initial and boundary conditions we have $\eta(0, t) = 1$, which is fixed in the simulations. Let $\mathcal{T}_h$ be a partition of the domain Ω with elements indicated by K, where h is the element characteristic length. Consider a typical finite element space V_h formed by functions $v_h \in C(\bar{\Omega})$ which are linear for each K and $v_h(0) = 0,\ \forall K \in \mathcal{T}_h$. Using basis $\{\varphi_i\}_{i=1}^m$ of hat functions on V_h, we define M and F as

$$M_{ij} = \langle \varphi_i, \varphi_j \rangle, \quad F_i = V_T \bar{u} \left\langle \rho\theta, \frac{\partial \varphi_i}{\partial x} \right\rangle - \frac{1}{\mathrm{Pe}_T} \left\langle \frac{\partial \theta}{\partial x}, \frac{\partial \varphi_i}{\partial x} \right\rangle + \langle \Phi, \varphi_i \rangle, \quad i = 1, 2, \ldots, m, \tag{35}$$

$$M_{(m+i)(m+j)} = \langle \varphi_i, \varphi_j \rangle, \quad F_{m+i} = \langle \Phi, \varphi_i \rangle, \quad i = 1, 2, \ldots, m. \tag{36}$$

We are interested in an approximate solution with the form

$$\theta_h(x, t) = \sum_{j=1}^{m} \alpha_j(t) \varphi_j(x), \quad \eta_h(x, t) = \varphi_0(x) + \sum_{j=1}^{m} \alpha_{m+j}(t) \varphi_j(x), \tag{37}$$

where φ_0 is a function describing left boundary and $\alpha : [0, \infty[\to \mathbb{R}^{2m}$ satisfies the semi-discrete problem

$$M\alpha'(t) = F(\alpha(t)), \quad t > 0, \qquad \alpha(0) = \alpha^0. \tag{38}$$

Vector α^0 provides initial solution $(\theta_h(\cdot, 0), \eta_h(\cdot, 0))$ equal to $(\theta_0(\cdot), \eta_0(\cdot))$ at nodal points of $\mathcal{T}_h$. Time discretization for nonlinear System (38) uses Crank–Nicolson scheme resulting in a discrete problem in time domain $[0, T]$. For each $k = 1, \ldots, n$, find $\alpha^k \in \mathbb{R}^{2m}$ such that $f^k(\alpha^k) = 0$, where

$$f^k(\alpha^k) = M(\alpha^k - \alpha^{k-1}) - \frac{\Delta t_k}{2}(F(\alpha^k) + F(\alpha^{k-1})). \tag{39}$$

The basis used in this work satisfies the property $\theta_h \geqslant 0, \eta_h \geqslant 0 \Leftrightarrow \alpha \geqslant 0$, where $\geqslant$ is considered for every vector component. This property allows us to obtain a complementarity formulation of the discrete problem: find $\alpha^k \in \mathbb{R}^m$, for each $k = 1, \ldots, n$, such that $\alpha^k \geqslant 0$, $f^k(\alpha^k) \geqslant 0$ and $f^k(\alpha^k) \bullet \alpha^k = 0$.

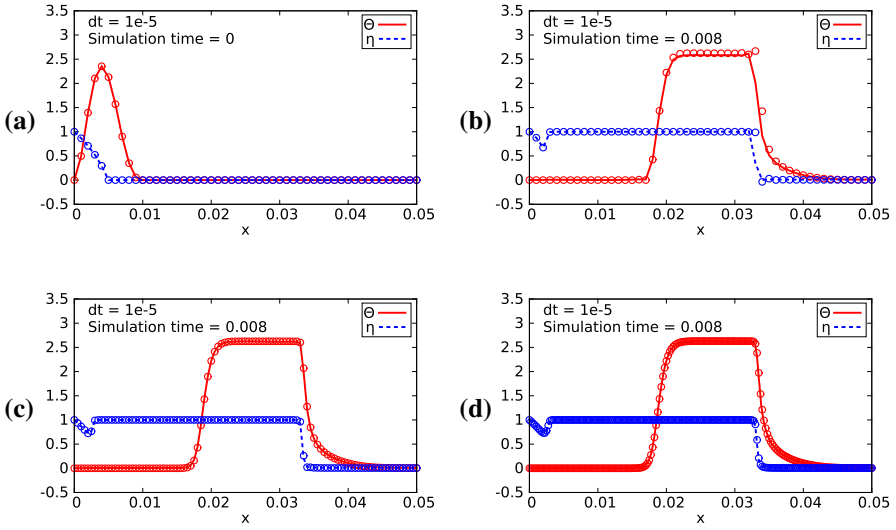

Fig. 4 Solution obtained with FEM+FDA-NCP (*lines*) is compared to one obtained with Crank–Nicolson+FEM (*circles*). Initial conditions are plotted in (**a**). Solution at time $t = 0.008$ are shown in (**b**), (**c**) and (**d**) corresponding to grids with 51, 101 and 201 points

Table 4 Relative errors for simulations using FEM

Method	Variable	Error 1	Error 2	Error 3
FDA	θ/η	0.666/0.580	0.081/0.072	0.034/0.044
CN+Newton	θ/η	0.164/0.107	0.072/0.059	0.022/0.026

See Sect. 5.1 for more details

In order to validate the implementation, we compare FEM simulations using FDA-NCP with direct numerical simulations using FEM discretization in space variable and Crank–Nicolson scheme in time. Newton's method is used in each time step to solve the nonlinear equation.

Our numerical simulations use the same parameter values, mesh size, time step and initial conditions as in Sect. 5. Following the same order as in Sect. 5.1, the simulation results are presented for space grids with 51 ($k = 10^{-5}$), 101 ($k = 5 \times 10^{-6}$) and 201 ($k = 2.5 \times 10^{-6}$) points; see Fig. 4b–d, respectively. We perform the same relative error analysis as described in Sect. 5.1, and the results are shown in Table 4. Notice that for FEM the relative error for discretization with more that 200 grid points reached the roundoff error.

Analyzing Figs. 3 and 4, one can realize that the wave speeds resulting from simulations with both methods are slightly different. In order to compare simulation results using FDS and FEM, we plot the distance between them for simulations taking 50-, 100-, 200- and 400-point grid at each time step in Fig. 5. The oscillations observed for 50-point grid are due to low quality of FDS solution. As it can be observed, both solutions goes to the same result when the grid is refined. As it can be noticed from Tables 3 and 4, the relative error decreases faster for simulations using FEM than those using FDS when refined grid was used.

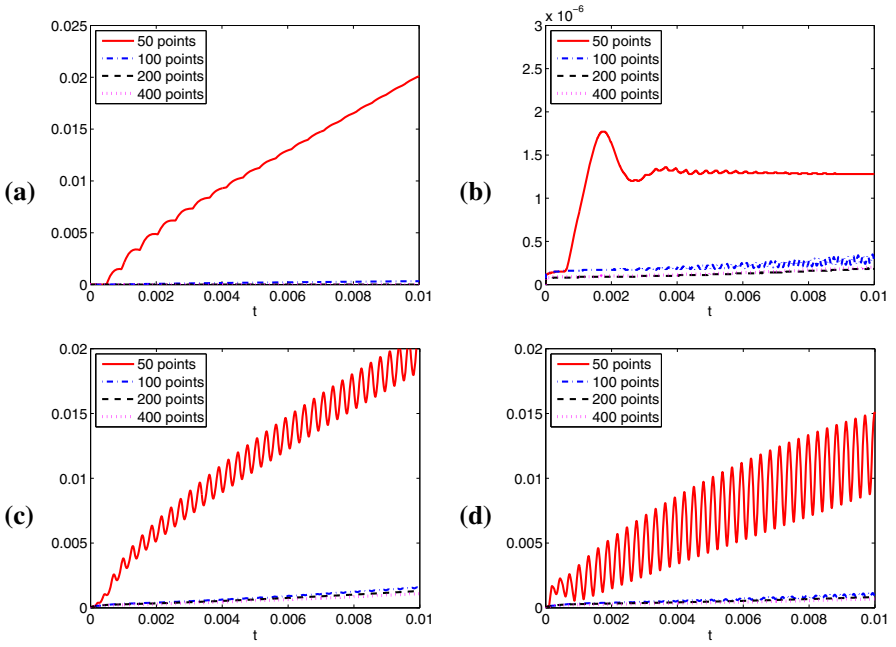

Fig. 5 Distance between solutions using FDS + FDA-NCP and FDS + Newton's method for variables θ (**a**) and η (**b**). The same using FEM + FDA-NCP and FEM + Newton's method for variables θ (**c**) and η (**d**)

5.3 Global Convergence

Let us first analyze the algorithm using FDS as presented in Sect. 5.1. Notice that for small Δt the discrete operator F_Δ from (30)–(32) can be rewritten as

$$F_\Delta(\theta^{n+1}, \eta^{n+1}) = \left[\theta_m^{n+1}, \eta_m^{n+1}\right]^T - \left[\theta_m^n, \eta_m^n\right]^T + O(\Delta t). \tag{40}$$

Let us check the three assumptions presented in Sect. 2.1.

1. In order to verify the conditions $u > 0$, $F(u) > 0$ (corresponding to $\theta > 0$, $\eta > 0$, $F_\Delta^1 > 0$, $F_\Delta^2 > 0$) for $u \in \Upsilon_c$, we proceed as follows. We chose the starting point u^0 satisfying these conditions. This is always possible for small Δt because of the form of the operator F_Δ in (40). Notice that F is continuous and then there exist a vicinity Υ_{u_0} of u^0 such that $u > 0$ and $F(u) > 0$ in this vicinity. Taking Δt as small as necessary, the potential function Φ is approximately quadratic. We choose c in such form that $\Upsilon_c \subset \Upsilon_{u_0}$. Notice that the set Υ_c is compact. This argumentation is valid for small Δt. During the simulation, the feasibility is checked at each time step.
2. The operator F_Δ in a discrete form given by (30)–(32) is regular and consequently satisfies the Lipschitz condition.

3. The matrix $diag(F(u)) + diag(u)\nabla F(u)$ is invertible in Υ_c^0 for small Δt because of the positiveness of the function F and the approximated form of F_Δ from (40).

Notice that these hypotheses are valid for the oxygen diffusion problem from Sect. 3, the calculations are analogous. In all the iterations, the FDA-NCP algorithm obtains a line search step going to 1 near the resolution. As stated in Sect. 2.1, this fact indicates that the FDA-NCP algorithm converges quadratically to the solution of the problem.

6 Conclusions

We propose a numerical method based on a nonlinear complementarity algorithm which can be applied to parabolic problems with moving boundary that appear in many applications. The main advantage in using the complementarity algorithm is the fact that the moving boundary is obtained directly as a solution of the complementarity problem. This approach has a potential advantage over the Newton's method where the moving boundary is difficult to obtain due to discontinuities of the solution. FDA-NCP is a simple, efficient and robust algorithm for nonlinear complementarity problems and converged for all time steps in all test problems.

To illustrate this idea, we apply this technique to two different examples. The oxygen diffusion problem is addressed in many works. Our results plotted in Fig. 1 and presented in Table 1 show good agreement with the literature.

In situ combustion was modeled using complementarity formulation with moving boundary, which can be an interesting approach for general flow in porous medium. Our numerical results show good agreement with direct numerical simulations using Newton's method combined with Crank–Nicolson FDS and FEM as shown in Figs. 3 and 4. The non-combustion waves that were obtained numerically are very similar to those given by the analytical study presented in Sect. 4.1. All the test problems were satisfactorily solved without the need of parameter tuning.

Acknowledgments The authors thank Prof. Jean R. Roche and anonymous referees for helping to improve the text. This work was supported in part by Conselho Nacional de Desenvolvimento Científico e Tecnológico (CNPq) and Fundação de Amparo à Pesquisa do Estado do Rio de Janeiro (FAPERJ).

References

1. Crank, J.: Free and Moving Boundary Problems. The Universities Press, Oxford (1984)
2. Ferris, M., Pang, J.: Engineering and economic applications of complementarity problems. SIAM Rev. **39**(1), 669–713 (1997)
3. Strikwerda, J.C.: Finite Difference Schemes and Partial Differential Equations. Wadsworth & Brooks, Belmont (1989)
4. Mazorche, S., Herskovits, J.: A new interior point algorithm for nonlinear complementarity problems. In: Proceedings of 6 World Congress on Structural and Multidisciplinary Optimization. Rio de Janeio, Brasil (2005)
5. Chapiro, G., Mazorche, S.R., Herskovits, J., Roche, J.R.: Solution of the nonlinear parabolic problem using nonlinear complementarity algorithm (fda-ncp). In: Mecánica Computacional, vol. XXIX, 20, pp. 2141–2153 (2010)
6. Gharbia, I.B., Jaffré, J.: Gas phase appearance and disappearance as a problem with complementarity constraints. Math. Comput. Simul. **99**, 28–36 (2014)

7. Chen, C., Mangasarian, O.: A class of smoothing functions for nonlinear and mixed complementarity problems. Comput. Optim. Appl. **5**(2), 97–138 (1996)
8. Lauser, A., Hager, C., Helmig, R., Wohlmuth, B.: A new approach for phase transitions in miscible multi-phase flow in porous media. Adv. Water Resour. **34**(8), 957–966 (2011)
9. Gupta, S.C.: The Classical Stefan Problem: Basic Concepts, Modelling and Analysis. Elsevier, Amsterdam (2003)
10. Herskovits, J.: A feasible directions interior point technique for nonlinear optimization. J. Optim. Theory Appl. **99**(1), 121–146 (1998)
11. Mazorche, S., Herskovits, J.: A feasible directions algorithm for nonlinear complementarity problems and applications in mechanics. Struct. Multidiscip. O. **37**(5), 435–446 (2009)
12. Morton, K., Mayers, D.: Numerical Solutions of Partial Differential Equations, 2nd edn. Cambridge University Press, Cambridge (2005)
13. Chapiro, G., Mailybaev, A.A., Souza, A., Marchesin, D., Bruining, J.: Asymptotic approximation of long-time solution for low-temperature filtration combustion. Comput. Geosci. **16**, 799–808 (2012)
14. Bruining, J., Mailybaev, A., Marchesin, D.: Filtration combustion in wet porous medium. SIAM J. Appl. Math. **70**, 1157–1177 (2009)
15. Crank, J., Gupta, R.: A moving boundary problem arising from the diffusion of oxygen in absorbing tissue. IMA J. Appl. Math. **10**(1), 19–33 (1972)
16. Gupta, R., Kumar, D.: Variable time step methods for one-dimensional Stefan problem with mixed boundary condition. Int. J. Heat Mass Transf. **24**, 251–259 (1981)
17. Ahmed, S.: A numerical method for oxygen diffusion and absorption in a sike cell. Appl. Math. Comput. **173**(1), 668–682 (2006)
18. Boureghda, A.: Numerical solution of the oxygen diffusion in absorbing tissue with a moving boundary. Commun. Numer. Methods Eng. **22**(9), 933–942 (2006)
19. Çatal, S.: Numerical approximation for the oxygen diffusion problem. Appl. Math. Comput. **145**(2–3), 361–369 (2003)
20. Gupta, R., Banik, N.: Approximate method for the oxygen diffusion problem. Int. J. Heat Mass Transf. **32**(4), 781–783 (1989)
21. Hansen, E., Hougaard, P.: On a moving boundary problem from biomechanics. IMA J. Appl. Math. **13**(3), 385–398 (1974)
22. Baiocchi, C., Pozzi, G.: An evolution variational inequality related to a diffusion–absorption problem. Appl. Math. Optim. **2**(4), 304–314 (1975)
23. Baiocchi, C., Capelo, A.: Variational and Quasivariational Inequalities: Applications to Free Boundary Problems. Wiley, London (1984)
24. Gupta, R.S.: Ph.D. thesis, Brunel University (1973)
25. Akkutlu, I., Yortsos, Y.: The dynamics of in-situ combustion fronts in porous media. Combust. Flame **134**, 229–247 (2003)
26. Chapiro, G., Bruining, J.: Enhanced recovery of shale gas through combustion. J. Petrol. Sci. Eng. **127**, 179–189 (2015)
27. Wahle, C., Matkowsky, B., Aldushin, A.: Effects of gas-solid nonequilibrium in filtration combustion. Combust. Sci. Technol. **175**, 1389–1499 (2003)
28. LeVeque, R.J.: Numerical Methods for Conservation Laws, vol. 132. Springer, Berlin (1992)
29. Chapiro, G., Marchesin, D., Schecter, S.: Combustion waves and Riemann solutions in light porous foam. J. Hyperb. Differ. Equ. **11**(02), 295–328 (2014)
30. Johnson, C.: Numerical Solution of Partial Differential Equations by the Finite Element Method. Cambridge University Press, Cambridge (1987)